

ground robot uses the center of these images—corresponding to the aerial robot’s projected ground position—as a dynamic navigation anchor, allowing it to follow the aerial path even when the target object is temporarily out of view.

The main contributions of this paper are as follows:

- 1) A hierarchical MA-LLM framework for aerial-ground robotic systems, where the aerial robot provides global semantic guidance through bird-view images, and the ground robot performs local navigation and manipulation by implicitly following the aerial path. This system bridges high-level reasoning and low-level execution, enabling adaptive task performance in dynamic environments.
- 2) An LLM-guided reasoning framework that performs two critical functions: hierarchical task decomposition and global semantic map construction. The LLM decomposes high-level user commands into executable sub-tasks and constructs a comprehensive global semantic map by integrating spatial-semantic information collected from multiple viewpoints, which serves as the basis for aerial path planning.
- 3) A VLM-driven perception strategy enhanced by GridMask-based fine-tuning, enabling accurate 2D localization and semantic labeling from bird-view images without depth sensing. The VLM extracts task-relevant semantic representations in real time, providing essential input for both global map construction and robots’ motion planning.
- 4) Extensive real-world experiments validate the effectiveness of our hierarchical MA-LLM framework in dynamic, long-horizon tasks. Using a heterogeneous aerial-ground robotic system, we demonstrate robust semantic navigation, precise manipulation, and coordinated behavior through letter-block assembly tasks, highlighting the system’s adaptability and decision-making capabilities in complex real-world scenarios.

II. RELATED WORKS

A. Heterogeneous Multi-Robot Systems

HMRS leverages diverse agent capabilities to address complex tasks. One of the earliest works in this area is Parker’s ALLIANCE architecture [9], which introduced fault-tolerant behavior-based coordination. Follow-up studies examined distributed task allocation and coordination [10], [11]. Recent methods also integrate deep multi-agent reinforcement learning to improve scalability and adaptability in decentralized settings [12].

In contrast to these approaches, our hierarchical MA-LLM framework offers a novel solution that bridges task decomposition, semantic perception, and low-level control. It addresses core challenges in HMRS, including flexible task allocation, semantic-aware motion planning, and precise manipulation.

B. Task Planning with Large Language Models

LLMs have enabled robots to decompose natural language into action plans, as demonstrated in SayCan [13], Prog-

Prompt [14], and RT-X [15]. These approaches effectively translate high-level user instructions into executable skills within constrained settings. Additionally, [16] further demonstrated that long-horizon task execution can be improved through human-robot collaboration.

Building on these advances, our method integrates LLMs not only for hierarchical task decomposition but also for global semantic map construction by aggregating aerial observations. This extension enables long-horizon semantic reasoning and effective multi-agent coordination in dynamic environments.

C. Vision-Language Models for Robotic Perception

General-purpose VLMs, such as CLIP [17] and Vision Transformers [18], effectively bridge visual inputs and semantic understanding. However, these models typically lack precise spatial reasoning capabilities needed for robotic applications. On the other hand, specialized models like RT-2 [19] integrate action grounding directly into Vision-Language-Action (VLA), enabling end-to-end robot control, yet they still face challenges in accurate localization.

Our approach addresses these limitations by employing GridMask-based fine-tuning, enhancing the VLM’s 2D localization and semantic labeling performance. This method supports both global semantic mapping and local navigation and manipulation tasks in aerial-ground robotic systems.

III. METHODS

To enable reliable task execution in our aerial-ground robotic system, we adopt a hierarchical MA-LLM framework. As illustrated in Fig. 2, the system is organized into three functional layers: a reasoning layer for task decomposition and allocation, and global map construction, a perceptual layer that extracts semantic understanding from aerial imagery, and an execution layer that performs robot actions through motion functions grounded in the reasoning and perception outputs.

The framework consists of the following components:

- *LLM-based reasoning layer*: Interprets natural language commands, decomposes them into structured sub-tasks, and selects appropriate motion functions for each robot. It also constructs and updates a global semantic map by integrating spatial-contextual information gathered during execution.
- *VLM-based perceptual layer*: Analyzes GridMask-enhanced aerial images to extract object-level semantics, including positions, orientations, and categories. These semantic cues provide environmental context for both initial mapping and real-time navigation support.
- *Execution layer*: Executes motion functions selected by the reasoning layer, each corresponding to a decomposed sub-task. These functions dynamically interact with the perceptual layer to obtain task-specific semantic information. For example, in global map construction, this layer gathers local semantic maps for global map integration by the reasoning layer; during local navigation and manipulation, local semantic information

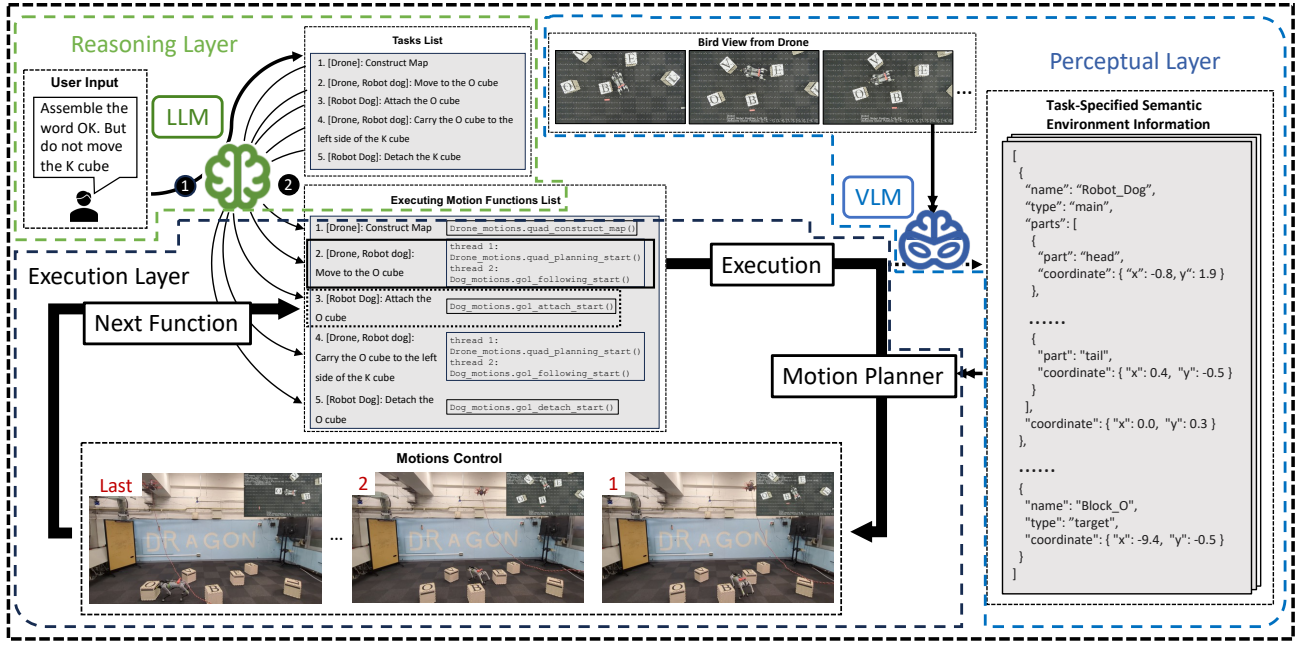


Fig. 2. An overview of the workflow for a long-horizon task using the hierarchical MA-LLM framework. The task starts with the instruction: “Assemble the word OK, but do not move K.” 1) The LLM decomposes the command and maps sub-tasks to motion functions for the aerial and ground robots. 2) The aerial robot visits multiple viewpoints to collect local maps, which the LLM integrates into a global semantic map. 3) Once the map is ready, both robots coordinate to reach the “O” cube. 4) The aerial robot follows a task-specific global path, while the VLM processes GridMask-enhanced bird-view images. 5) The ground robot uses this semantic input from the VLM to complete its assigned sub-task via local planning.

is extracted in real-time to guide ground motions. This layer acts as the bridge between high-level plans and grounded actions, coordinating aerial-ground behaviors across perception and reasoning.

A. LLM-based Reasoning Layer Design

To enhance the reasoning capability of the LLM-based layer, we design task-specific prompts tailored to its functional responsibilities within the aerial-ground robotic system. The summarized prompts are as follows:

1) *Task decomposition and allocation*: To enable reasoning across heterogeneous agents, we adopt a role-specific prompt design. The LLM is instructed to act as a task decomposer and allocator, mapping high-level goals to robot-specific sub-tasks based on their capabilities.

```
# Duty clarify
You are a task decomposer and allocator for a heterogeneous multi-robot system. Decompose complex tasks into sub-tasks for each robot according to their abilities.

# Robots' abilities
- Drone:
  1. Construct the map. (Must be the first step before other sub-tasks)
- Robot Dog:
  1. Attach/Detach to an object.
- Drone and Robot Dog Cooperation:
  1. Move to a specified location.
  2. Carry an object to a specified location.
```

2) *Motion functions mapping*: To ensure the LLM generates executable action plans, we provide the available motion functions for each robot via the prompt. This prevents invalid actions and constrains the reasoning process to grounded,

system-supported functions.

```
# Duty clarify
You are responsible for choosing the motion function to finish the task.

# Robots' motion functions
- Drone:
  1. quad_construct_map()
- Robot Dog:
  1. gol_attach_start("name_of_target_object")
  2. gol_detach_start("name_of_target_object")
- Drone and Robot Dog Cooperation:
  Thread 1: drone.quad_planning_start("task")
  Thread 2: dog.gol_following_start("task")
```

3) *Global semantic map integration*: These chain-of-thought prompts are used to improve the model’s ability to analyze local maps and construct a global map.

```
# Duty clarify
You need to construct a global map by logically integrating all provided local map data.

# Chain-of-thought
- Cross-map Validation:
  1. Always cross-check objects across multiple local maps; do not rely on a single observation.
- Error Identification:
  1. Detect and exclude erroneous entries.
  2. If an object is only present in a single local map and absent from others, where logically it should be visible, remove it.
- Conflict Resolution:
  1. If objects appear unrealistically close, identify the mislabeled object and correct or remove it.
  2. Resolve conflicting labels by majority voting across maps or flags.
- Synonym Handling
```

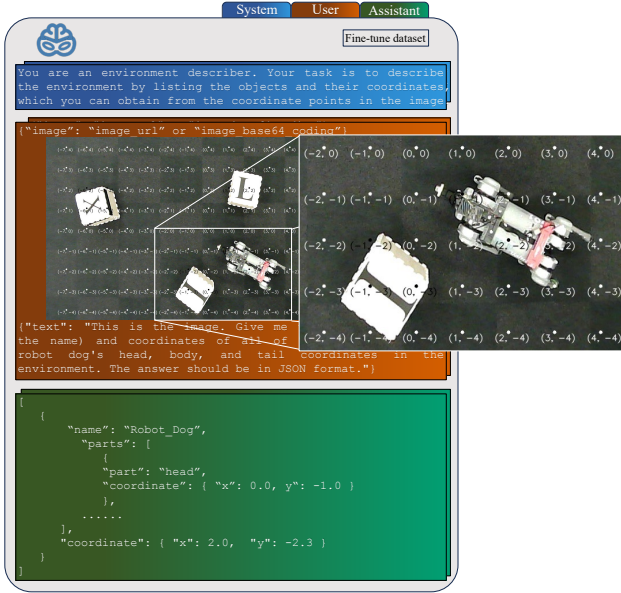


Fig. 3. An illustration of the fine-tuning dataset, showing the system prompt, user instruction with GridMask-based image input, and the layer’s ideal output in structured JSON format.

This layer serves as the top-level reasoning layer, translating user commands into modular functions for downstream execution.

B. VLM-based Perceptual Layer Design

To enhance the perceptual capabilities of the VLM-based layer, we employ prompt engineering and fine-tune the model using a task-specific visual dataset annotated with GridMask.

We design role-specific prompts to guide the VLM in outputting structured environmental information clearly and accurately:

```
# Duty Clarification
You are an environment describer and classifier.
Your task is to identify all objects in the
environment, provide their names and coordinates
in a structured JSON format, and classify them
according to the provided task requirements.

# Detailed Instructions
- The environment is overlaid with a dense
coordinate grid, with the origin at the center.
The x-axis extends horizontally from left to
right, and the y-axis extends vertically from
bottom to top. The coordinate (0, 0) represents
the central reference point.
- Depending on the given task, classify
each object by labeling it into one of four
categories: main, target, landmark, or obstacle.
- Important Note:
  1. For local navigation tasks, do not use
global coordinates directly. Instead, if the task
involves moving to a specified global coordinate
(XX, XX), set this target as (0, 0) to indicate
that the ground robot should follow relative
movements guided by the aerial robot.
  2. For map construction, you do not need to
make the labeling classification.
```

While prompts guide the VLM’s response format and labeling logic, spatial localization remains a challenge. To address this, we introduce GridMask—a structured visual cue

that overlays a dense coordinate grid on bird-view images captured by the aerial robot. Each grid cell measures 80×80 pixels, offering a balance between spatial resolution and semantic clarity. As shown in Fig. 3, this approach allows the VLM to associate visual features with absolute 2D coordinates in a data-driven manner.

Based on this structured GridMask, we fine-tune the VLM on a dataset pairing textual descriptions with corresponding object coordinates and orientations. After fine-tuning, the VLM provides robust zero-shot identification of objects’ spatial positions and roles, classified as follows:

- **main:** The primary agent performing the task, typically the ground robot. Objects carried by the robot are also labeled main.
- **target & landmark:** target denotes the direct goal position; landmark serves as a spatial reference, further classified into four directional indicators (front, back, left, and right).
- **obstacle:** Objects obstructing motion paths. Landmarks may simultaneously serve as obstacles during task execution.

A detailed structure of the fine-tuning dataset and annotation process is also depicted in Fig. 3.

Serving as the perceptual layer, it provides structured semantic observations that support and ground high-level plans.

C. Execution Layer Design - Motion Functions Pre-Programming

Acting as the executing layer, it bridges the reasoning and perceptual layers, ensuring the execution of low-level motion functions. To realize this execution, we define a set of pre-programmed motion functions that enable task-level behaviors in the aerial-ground robotic system, as described below.

1) *Aerial robot - Global semantic map construction:* The `quad_construct_map()` function enables high-level spatial understanding by fusing perception, motion context, and language reasoning. It serves as the semantic foundation for downstream planning by generating a global map from aerial image observations. The process consists of the following steps and is illustrated in Fig. 4:

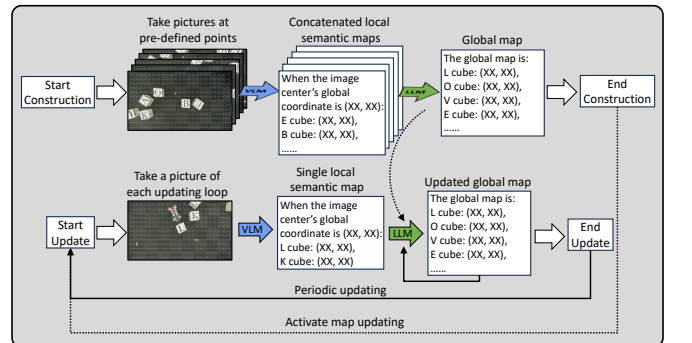


Fig. 4. Workflow of the `quad_construct_map()` function. Local semantic maps derived from aerial images are integrated by the LLM to form a semantic map, which is subsequently updated at a fixed frequency during task execution.

- **Local Map Generation:** The aerial robot executes a predefined waypoint path to collect bird-view images. Each image is processed by the VLM to produce local semantic maps containing object classes and positions.
- **Global Map Integration:** The LLM receives a concatenated textual representation of all local semantic maps and infers a spatially consistent global map. This process involves cross-map validation, confidence reasoning, and label disambiguation. The global map will keep updating during task execution.

2) *Aerial robot - Global path planning:* As the leader in the aerial-ground robotic system, the aerial robot plans a globally optimal path that not only avoids obstacles but also dynamically guides the ground robot. The function `quad_planning_start()` enables autonomous navigation and obstacle avoidance by generating a collision-free path from a global semantic map. This path guides the ground robot by defining a dynamically updated spatial target (zero point), allowing it to follow the aerial robot through task-relevant areas with global awareness.

Given the semantic map from the LLM and object classification from the VLM (`type: target, main, obstacle, landmark`) with their coordinates (`coordinate`), the system constructs a task-specific cost function for global path optimization. This path ensures smoothness and collision avoidance through spline interpolation and constraint minimization techniques. Details of this optimization are described mathematically below.

Spline Path Generation: The initial path is defined by control points interpolated using B-splines to ensure smooth trajectories. Control points $\mathbf{C} = \{\mathbf{c}_0, \mathbf{c}_1, \dots, \mathbf{c}_n\}$ are initially placed along a straight line connecting the `main` to the `target` or guided toward a specified `landmark`. This approach provides a straightforward and feasible initial path for subsequent optimization. The B-spline $\mathbf{S}(u)$ is formulated as:

$$\mathbf{S}(u) = \sum_{i=0}^n N_{i,k}(u) \mathbf{c}_i, \quad u \in [0, 1], \quad (1)$$

where $N_{i,k}(u)$ are the B-spline basis functions of degree k .

Cost Function Formulation: The optimization aims to minimize a cost function J that balances path length, smoothness, and obstacle avoidance. The cost function is defined as:

$$J_{\text{global}} = Q_L L(\mathbf{C}) + Q_K K(\mathbf{C}) + Q_{O_{\text{global}}} O_{\text{global}}(\mathbf{C}), \quad (2)$$

where:

- $L(\mathbf{C})$: The cost of total path length, penalizes the overlength of the path

$$L = \sum_{i=1}^m \|\mathbf{S}(u_i) - \mathbf{S}(u_{i-1})\|. \quad (3)$$

- $K(\mathbf{C})$: The cost of path curvature, promoting the smoothness of the path.

$$K = \sum_{i=2}^{m-1} \|\mathbf{S}(u_{i+1}) - 2\mathbf{S}(u_i) + \mathbf{S}(u_{i-1})\|. \quad (4)$$

- $O_{\text{global}}(\mathbf{C})$: The cost of obstacle avoidance. For each obstacle \mathbf{o}_j in N and each sampled point $\mathbf{S}(u_i)$ in m , the penalty is applied if the distance is less than d_{safe} .

$$O_{\text{global}}(\mathbf{C}) = \sum_{j=1}^N \sum_{i=1}^m \max(0, d_{\text{safe}} - \|\mathbf{S}(u_i) - \mathbf{o}_j\|)^2. \quad (5)$$

- $Q_L, Q_K, Q_{O_{\text{global}}}$ are weighting coefficients balancing the respective components.

Optimization Constraints: The optimization is subject to boundary conditions that fix the start and end points of the path.

Optimization Procedure: The optimized control points \mathbf{C}^* are obtained by minimizing the cost function J :

$$\mathbf{C}^* = \arg \min_{\mathbf{C}} J_{\text{global}}. \quad (6)$$

This optimized path forms the basis for semantic guidance, with the aerial robot's ground-projected position serving as a continuously updated local navigation anchor for the ground robot.

3) *Ground robot - Local semantic navigation and manipulation:* Acting as the follower in the aerial-ground system, the ground robot performs iterative local navigation that is continuously coupled to the aerial robot's projected path and semantic observations. This process is implemented through `gol_following_start()`, which continuously guides the robot using semantic inputs from the aerial robot.

At each time step, the robot generates a set of candidate velocity directions θ uniformly distributed over 360° , and evaluates them using a cost function that reflects goal alignment, obstacle avoidance, and environmental constraints.

The semantic input for this local planning is derived from the VLM, which processes bird-view images to generate a task-specified local semantic map centered at the aerial robot's projection point. The map includes object-level annotations (`type: target, main, obstacle, landmark`) and part-level annotations for the ground robot (`parts: head, body, tail`) with their coordinates (`coordinate`). These annotations allow the system to estimate the robot's current orientation and target-relative position in the local frame.

Inspired by the classical Dynamic Window Approach (DWA) [20], we compute the cost for each candidate direction θ using a semantically-augmented weighted function:

$$J_{\text{local}}(\theta) = Q_A A(\theta) + Q_{\text{zero}} A_{\text{zero}}(\theta) + Q_{O_{\text{local}}} O_{\text{local}}(\theta) + Q_W W(\theta), \quad (7)$$

where each term is defined as follows:

- $A(\theta)$: penalizes angular deviation from the direct path toward the target object, encouraging goal-oriented motion.
- $A_{\text{zero}}(\theta)$: encourages alignment towards the aerial robot's projected position at coordinate frame center $(0,0)$, reinforcing the leader-follower coordination.

- $O_{\text{local}}(\theta)$: represents the obstacle proximity penalty, calculated explicitly as:

$$O_{\text{local}}(\theta) = \sum_{O \in \mathcal{O}} \begin{cases} \frac{1}{d_{\perp}(O, \theta) + \epsilon}, & \text{if } d_{\perp}(O, \theta) < d_{\text{safe}}, \\ 0, & \text{otherwise,} \end{cases} \quad (8)$$

where $d_{\perp}(O, \theta)$ is the perpendicular distance from the obstacle O to the robot's projected path along the candidate direction θ , d_{safe} defines a safety margin, and ϵ prevents division by zero. This explicit formulation ensures rapid penalty increase near obstacles, strongly discouraging unsafe paths.

- $W(\theta)$: enforces boundary constraints, assigning infinite cost to directions that exceed the local images' margin.
- $Q_A, Q_{\text{zero}}, Q_{O_{\text{local}}}, Q_W$ are weighting coefficients balancing the respective components.

At each iteration, the robot selects the optimal direction θ^* minimizing the combined cost:

$$\theta^* = \arg \min_{\theta_i} J_{\text{local}}(\theta_i), \quad (9)$$

and adjusts its orientation accordingly. The robot moves forward or backward based on the relative position of the target in its local coordinate frame, calculated using semantic annotations. The iterative process terminates once both positional (distance to target below a predefined threshold) and orientation alignment (within a certain angular tolerance) criteria are met.

Through this mechanism, the ground robot adaptively navigates toward the target while remaining tightly coupled to the semantic path defined by the aerial robot.

4) *Ground robot - Attach and detach*: The ground robot is equipped with a servo-driven magnetic attachment device featuring a mechanical toggle switch. This device allows the robot to attach to or detach from objects located in front of it, enabling versatile interactions with its environment. By using function `gol_attach_start()` and `gol_detach_start()` to control the servo to actuate the switch, toggling between attachment and detachment.

IV. EXPERIMENTS AND DISCUSSION

We evaluate the proposed system along two axes: 1) the effectiveness of the GridMask-based VLM fine-tuning

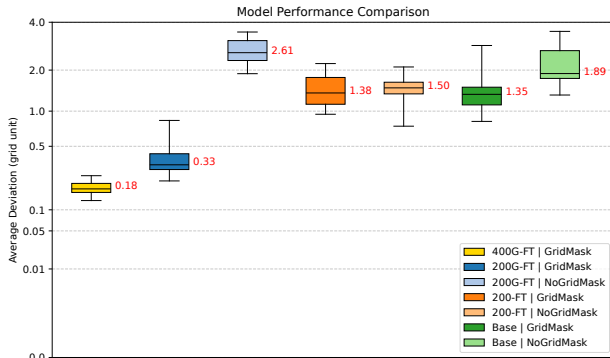


Fig. 5. Performance comparison of different models based on objects' average Euclidean deviation from ground-truth positions in the image (in grid units).

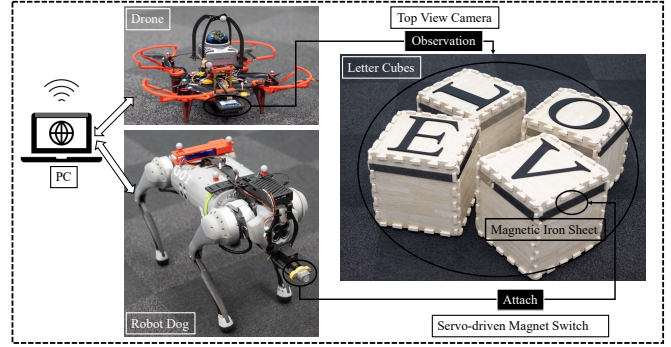


Fig. 6. Hardware setup of the aerial-ground robotic system, illustrating how the drone and ground robot cooperate to pick, transport, and place target objects.

in improving semantic perception; and 2) the real-world performance of the aerial-ground robotic system in different reasoning tasks.

A. Experiment for the GridMask-based tuning

The objective of this experiment is to evaluate the effectiveness of the GridMask-based fine-tuning approach. The Gemini-flash-1.5-002 model was used in this study, and four groups of models were tested under different fine-tuning and input conditions, but the same origin image dataset (Number of epochs: 10; Learning rate multiplier: 1; Adapter size: 1):

- 1) 400G-FT | GridMask: model fine-tuned with 400 GridMask data, tested on images containing GridMask annotations.
- 2) 200G-FT | GridMask and NoGridMask: models fine-tuned with 200 GridMask data, tested on both images with and without GridMask annotations.
- 3) 200-FT | GridMask and NoGridMask: models fine-tuned with the 200 same image dataset but without GridMask annotations, tested on both images with and without GridMask annotations.
- 4) Base | GridMask and NoGridMask: The baseline model without fine-tuning, which was tested on both images with and without GridMask annotations.

The performance of the models was evaluated by measuring the Euclidean deviation between detected and ground truth object positions, with lower deviation values indicating better accuracy.

Fig. 5 summarizes the performance across different model groups, highlighting key findings: 1) Models consistently perform better on images with GridMask annotations, regardless of fine-tuning. This suggests that GridMask annotations inherently improve spatial perception. 2) The best performance, with a median deviation of around 0.15 units, is achieved by models trained and tested with GridMask annotations (400G-FT | GridMask). Additionally, increasing the number of training samples from 200G-FT to 400G-FT further enhances model accuracy. 3) Models fine-tuned with GridMask data (200G-FT) exhibit weaker performance when tested on non-GridMask images compared to models fine-tuned without GridMask data (200-FT), indicating reduced

TABLE I
QUANTITATIVE RESULTS: PERFORMANCE COMPARISONS WITHIN DIFFERENT TASK TYPES

Task Type	Metric	Trials per Task	Accuracy & Success Rate	
Type A: Simple Task (Direct Command)	Task Decomposition	5	1.00	
	Task Completion Success	5	0.80	
Type B: Simple Task (Reasoning Required)	Task Decomposition	5	0.80	
	Task Completion Success	5	0.80	
Type C: Complex Task (Long-Horizon Reasoning)	Task Decomposition	5	1.00	
	Task Completion Success	5	0.80	
Common Metrics		Trials in Total	Accuracy & Success Rate	Collisions Times
Global Map Construction Accuracy		15	0.87	—
Collisions Count		25	—	0.68
Recognition Accuracy		378	0.74	—
Semantic Labeling Accuracy		378	1.00	—

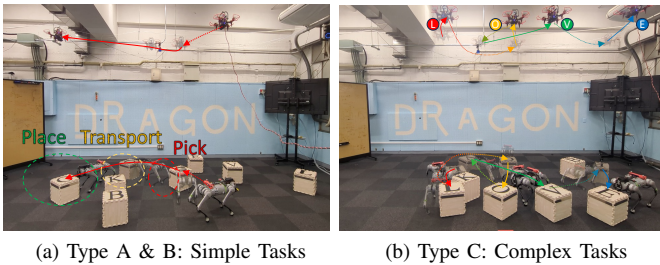


Fig. 7. Real-world experiments showing (a) execution of simple tasks (Type A & B) such as assembling “OK”, and (b) complex task (Type C) involving assembly of “LOVE”.

generalization capability due to dependency on GridMask annotations.

Overall, these results validate that GridMask annotations enhance spatial localization at the cost of generalization. To further improve real-world performance, we additionally trained a larger model (1000G-FT | GridMask) as the VLM, which is used in the subsequent real-world experiments.

B. Experiment for the real-world application

In a real-world application, the hierarchical MA-LLM framework is implemented in a ROS-based aerial-ground robotic system comprising a Unitree Go1 quadruped robot and a custom-designed quadrotor equipped with SLAM capabilities [21]. Fig. 6 presents the aerial-ground robotic system and the letter blocks, meanwhile how they interact with each other. A prompted Gemini-pro-2.0 model was used here as the LLM.

Our experiments aim to assess the system’s effectiveness in interpreting and executing complex user instructions in real-world scenarios. We specifically evaluate task decomposition, zero-shot detection, semantic labeling, and robotic planning and control.

The system was tested on various assembly tasks: 1) Type A: Simple tasks with a direct command like moving the “L” to the front side of the O cube. 2) Type B: Simple tasks that need reasonability, including the task of assembling words like “OK” or “BE” but do not move one of them. 3) Type C: Complex, long-horizon tasks requiring strategic arrangement (e.g., assembling the word “LOVE”, with flexible sequence and optional fixed cube positions). Representative examples

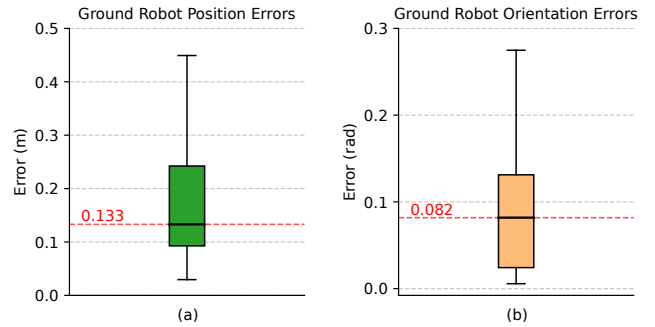


Fig. 8. (a) Position error distribution of the ground robot. (b) Orientation error distribution of the ground robot.

of Type A & B and Type C task executions are shown in Fig. 7.

In addition, we validate the zero-shot detection accuracy in real-world scenarios by comparing: a) the ground robot’s position error, calculated from aerial robot positions obtained via SLAM; b) The aerial robot’s yaw is fixed to zero and aligned with the world frame, allowing the ground robot’s yaw to be directly evaluated in that frame. As shown in Fig. 8, the median of the position error is approximately 0.13 m, and the median of the orientation error is around 0.08 rad. Apart from model errors, the observed deviations are primarily attributed to the aerial robot’s pose instability, which introduces transformation errors. In addition, residual lens distortion and projection inaccuracies contribute to spatial estimation error. While these errors pose challenges for precise manipulation, they remain within an acceptable range, as demonstrated by the successful task completion rates in Table I.

Furthermore, the real-world applicability of the system was evaluated using six key metrics, as summarized in Table I:

- **Task Decomposition Accuracy:** Evaluates the correctness of translating user instructions into robot-specific sub-tasks. Generally, the system demonstrated strong decomposition capabilities. However, failures occurred once with commands involving negation or implicit spatial constraints, such as misinterpreting the spatial relation in the instruction *assemble the word BE but do not move B*, incorrectly placing the E cube on the left instead of the right.

- **Task Completion Success:** Measures the degree to which the final robot arrangement matches the intended user commands, achieving an overall success rate of 80%. Two failures were due to inaccuracies in the global semantic map that impacted aerial path planning, with one case resulting from initial decomposition errors. This indicates robust task execution overall, though sensitive to upstream perceptual inaccuracies.
- **Global Map Construction Accuracy:** Assesses the accuracy (87%) in combining local semantic maps into a consistent global map. The system was effective in correcting overlapping labeling errors but struggled with errors in isolated local maps, highlighting its reliance on redundancy to maintain robustness.
- **Collisions Count:** Records the frequency of collisions (average of 0.68 per pick-transport-place operation). Note that this count also includes minor collisions or slight contacts. Collisions primarily resulted from errors in orientation estimation, motion control limitations, and residual projection inaccuracies, particularly in cluttered environments. Despite these challenges, the collision rate remains acceptably low, indicating effective semantic navigation performance.
- **Recognition Accuracy:** Quantifies the system’s capability to accurately identify object identities visually, achieving 74% accuracy. Recognition errors predominantly arose from visual ambiguities, particularly rotated cubes, leading to confusion between similar characters (e.g., confusing “L” and “T”).
- **Semantic Labeling Accuracy:** Evaluates the assignment accuracy of semantic labels (main, target, landmark, obstacle) after correct object recognition. The system achieved perfect labeling accuracy in all 378 trials, confirming reliable task-oriented labeling capability.

Overall, these experimental results demonstrate that our hierarchical MA-LLM framework effectively integrates semantic perception and reasoning, presenting robust real-world performance despite isolated challenges in perception accuracy and spatial reasoning.

V. CONCLUSION

This paper presents a hierarchical MA-LLM framework that integrates LLM-based task reasoning, VLM-based semantic perception, and motion-level execution for an aerial-ground heterogeneous robotic system. Through a structured three-layer design, the system interprets natural language commands, constructs semantic maps, and executes complex manipulation tasks via aerial-ground robots’ behaviors. Experiment results validate the effectiveness of GridMask-based fine-tuning in enhancing spatial perception accuracy and demonstrate the robustness of the hierarchical MA-LLM framework in complex manipulation scenarios. The system’s capability to perform adaptive local navigation and maintain aerial-ground alignment even in target-absent conditions highlights its applicability in real-world environments.

Future work will extend this framework to 3D motion planning, enhancing aerial robot navigation in unstructured spaces. Additionally, incorporating advanced multi-agent coordination strategies and expanding adaptive reasoning capabilities will further broaden the framework’s applicability to practical tasks such as search-and-rescue, warehouse automation, and industrial robotics.

REFERENCES

- [1] Z. Yan, N. Jouandeau, and A. A. Cherif, “A survey and analysis of multi-robot coordination,” *International Journal of Advanced Robotic Systems*, vol. 10, no. 12, p. 399, 2013.
- [2] M. Calvo-Fullana, M. Gerasimenko, D. Mox *et al.*, “A networked multiagent system for mobile wireless infrastructure on demand,” *IEEE Transactions on Robotics*, vol. 40, pp. 4598–4614, 2024.
- [3] M. Coppola, K. N. McGuire, C. De Wagter, and G. C. De Croon, “A survey on swarming with micro air vehicles: Fundamental challenges and constraints,” *Frontiers in Robotics and AI*, vol. 7, p. 18, 2020.
- [4] Y. Rizk, M. Awad, and E. W. Tunstel, “Cooperative heterogeneous multi-robot systems: A survey,” *ACM Computing Surveys (CSUR)*, vol. 52, no. 2, pp. 1–31, 2019.
- [5] OpenAI, “Gpt-4 technical report,” *arXiv*, 2024.
- [6] G. Team, “Gemini: A family of highly capable multimodal models,” *arXiv*, 2024.
- [7] J. Liang, W. Huang, F. Xia *et al.*, “Code as policies: Language model programs for embodied control,” *arXiv*, 2023.
- [8] I. Kapelyukh, Y. Ren, I. Alzugaray, and E. Johns, “Dream2real: Zero-shot 3d object rearrangement with vision-language models,” in *2024 IEEE International Conference on Robotics and Automation (ICRA)*, 2024, pp. 4796–4803.
- [9] L. Parker, “Alliance: an architecture for fault tolerant multirobot cooperation,” *IEEE Transactions on Robotics and Automation*, vol. 14, no. 2, pp. 220–240, 1998.
- [10] L. Iocchi, D. Nardi, M. Piaggio, and A. Sgorbissa, “Distributed coordination in heterogeneous multi-robot systems,” *Autonomous robots*, vol. 15, pp. 155–168, 2003.
- [11] G. Notomista, S. Mayya, S. Hutchinson, and M. Egerstedt, “An optimal task allocation strategy for heterogeneous multi-robot systems,” in *2019 18th European control conference (ECC)*. IEEE, 2019, pp. 2071–2076.
- [12] Y. Gao, J. Chen, X. Chen *et al.*, “Asymmetric self-play-enabled intelligent heterogeneous multirobot catching system using deep multiagent reinforcement learning,” *IEEE Transactions on Robotics*, vol. 39, no. 4, pp. 2603–2622, 2023.
- [13] M. Ahn, A. Brohan, N. Brown *et al.*, “Do as i can, not as i say: Grounding language in robotic affordances,” *arXiv*, 2022.
- [14] I. Singh, V. Blukis, A. Mousavian *et al.*, “Progprompt: Generating situated robot task plans using large language models,” in *2023 IEEE International Conference on Robotics and Automation (ICRA)*, 2023, pp. 11 523–11 530.
- [15] A. O’Neill, A. Rehman, A. Maddukuri *et al.*, “Open x-embodiment: Robotic learning datasets and rt-x models : Open x-embodiment collaboration0,” in *2024 IEEE International Conference on Robotics and Automation (ICRA)*, 2024, pp. 6892–6903.
- [16] H. Liu, Y. Zhu, K. Kato *et al.*, “Enhancing the llm-based robot manipulation through human-robot collaboration,” *IEEE Robotics and Automation Letters*, vol. 9, no. 8, pp. 6904–6911, 2024.
- [17] A. Radford, J. W. Kim, C. Hallacy *et al.*, “Learning transferable visual models from natural language supervision,” in *International conference on machine learning*. PMLR, 2021, pp. 8748–8763.
- [18] A. Dosovitskiy, L. Beyer, A. Kolesnikov *et al.*, “An image is worth 16x16 words: Transformers for image recognition at scale,” *arXiv*, 2020.
- [19] A. Brohan, N. Brown, J. Carbajal *et al.*, “Rt-2: Vision-language-action models transfer web knowledge to robotic control,” *arXiv*, 2023.
- [20] D. Fox, W. Burgard, and S. Thrun, “The dynamic window approach to collision avoidance,” *IEEE Robotics & Automation Magazine*, vol. 4, no. 1, pp. 23–33, 1997.
- [21] Y. Li, M. Zhao, J. Sugihara, and T. Nishio, “Cooperative navigation system of agv and uav with autonomous and precise landing,” in *2024 IEEE International Conference on Mechatronics and Automation (ICMA)*. IEEE, 2024, pp. 1477–1483.